Hybrid FRP Strengthening of Slender Steel Members for Buckling Control

Daina MacEachern[1] and Pedram Sadeghian[2]

ABSTRACT: In this paper, the structural properties and behaviour of slender steel members strengthened against buckling by a hybrid system of fibre-reinforced polymer (FRP) shells filled with self-consolidating grout (SCG), in the form of buckling restrained bracing (BRB), were investigated. The goal of the hybrid system is to increase the load carrying capacity of the slender member to reach the yielding load of the steel core through the addition of lateral support. A total of 36 small-scale specimens (27 strengthened specimens and 9 plain 25.4 mm×6.35 mm steel cores) were prepared and tested in compression. Strengthened specimens were prepared with three different FRP shell lengths (300, 600, and 900 mm) and three outer shell diameters (41, 53, and 65 mm). A lubricant was applied to the steel core to allow the steel core to carry the majority of the axial load independently. The contribution of each component of the hybrid system to the overall load carrying capacity was also calculated. The steel core was found to carry on average 86% of the load at yielding with the grout and FRP carrying only 13.5% and 0.5%, respectively. A simple linear elastic model was created to predict the failure mode of the hybrid system that can also be used to design an optimized system. The model accurately predicted the failure mode for all 27 reinforced specimens. Overall, provided the hybrid FRP strengthening system was sufficiently sized, the system was successful in changing the failure mode of the steel core from buckling to yielding.

DOI: https://doi.org/10.1061/(ASCE)CC.1943-5614.0001050

[1] Former MASc Student, Department of Civil and Resource Engineering, Dalhousie University, 1360 Barrington Street, Halifax, NS B3H 4R2, Canada. Email: D.MacEachern@dal.ca

[2] Assistant Professor and Canada Research Chair in Sustainable Infrastructure, Department of Civil and Resource Engineering, Dalhousie University, 1360 Barrington Street, Halifax, NS, B3H 4R2, Canada. Email: pedram.sadeghian@dal.ca (corresponding author)

KEYWORDS: Slender, Steel, Column, Bracing, Strengthening, FRP, Shell, Hybrid, BRB.

INTRODUCTION

Globally, the volume of infrastructure in need of repair or replacement is rapidly increasing (Porter and Lopez-Claros 2006; ASCE 2016; CSCE 2016; Schulze 2016; Schwab 2018; Tondo 2018). Efficient and economical solutions for improving the state of this infrastructure (e.g. buildings and bridges) is becoming more critical. Age, deteriorating conditions, and potential applied load changes to slender members, including columns, braces and piles, has led to various market solutions that improve resistance to buckling. Conventional methods of reinforcing slender members include bulking the structures up with additional material such as steel, concrete or fibre-reinforced polymer (FRP) composites (Wu and Grondin 2002; Ekiz and El-Tawil 2008; El-Tawil and Ekiz 2009; Harries et al. 2009; Sadeghian et al. 2009; Shaat and Fam 2009; Gao et al. 2013; Kim and Choi 2015; Vild and Bajer 2017). Recently, a more advanced method of increasing the buckling capacity of slender members was developed called a buckling restrained brace (BRB) (Black et al. 2004; Carden et al. 2004; Tremblay et al. 2006; Almeida et al. 2017). These are currently shop fabricated, field installed systems that consist of steel members encased in a steel tubing filled with concrete or mortar. For these systems to function properly a lubricant is applied to the steel member to allow free axial expansion and contraction by eliminating friction and shear transfer (Black et al. 2004). The BRB system is applicable for either adding additional bracing, fully replacing old bracing in existing structures, or for installing in new structures. These systems are currently custom-designed and manufactured for specific projects (Kersting et al. 2015). For cases where the existing bracing or column need to be kept and upgraded, the BRB system is not applicable.

The solution investigated in this paper is a hybrid system of an FRP shell and grout which can be applied in the field to the existing member to increase its buckling capacity. This method is like

the conventional BRB system but involves forming a shell out of a thin, pre-impregnated FRP laminate around members in the field instead of a steel shell fabricated in a shop that would require removal of the existing member to install. This hybrid system will be referred to as a fibre-reinforced polymer buckling restrained brace (FRP-BRB) system. For this system the FRP laminate is rolled into a cylindrical shape around the existing steel bracing with enough gap and held together with an adhesive. The shell then acts as formwork for the grout and remains as part of the structural system. Similar to the classic BRB system described previously; a lubricant is applied to the steel to allow its axial movement to be independent of the grout. The goal behind inhibiting bonding between the steel and grout is to ensure a ductile failure of the brace, as well as to avoid cracking of the grout in compression which would weaken the lateral support. Once the FRP shell is cured, it is filled with a cement-based self consolidating grout (SCG) or concrete (SCC). The desired outcome of this strengthening technique, when properly sized, is to provide lateral buckling support while allowing the restrained member to reach its yielding capacity. The purpose of the system is to restrain the core from buckling, not to provide confinement. The main goal of a BRB is to improve hysteretic energy dissipation capacity under cyclic loading (Black et al. 2004; Carden et al. 2004; Tremblay et al. 2006; Almeida et al. 2017). However, this paper will investigate a static model and study as a proof of concept. Further testing may include cyclic testing as well as larger scale specimens. It is noted that the concept of the FRP-BRB explored in this paper is as per U.S. Patent Number 9,719,255 B1 for buckling reinforcement for structural members (Ehsani 2017).

Currently the research on the topic of FRP-BRB's is limited with most of the research focused on conventional steel BRB's. There have been a few studies conducted on strengthening slender steel members using a concrete or grout filled FRP tube, however the majority of this research has allowed the filler material to bond directly to the steel (Liu et al. 2005; Han et al. 2010; Feng et al. 2013). The

goal of a BRB is to ensure the steel core yielding is the primary failure mode. This is achieved by limiting the transfer of load between the steel core and filler material (Black et al. 2004; Carden et al. 2004; Tremblay et al. 2006; Almeida et al. 2017). If a bond is allowed between the two, the load will be carried by the core, filler, and shell which may lead to a crushing failure of the filler or rupture of the shell. Many of the studied techniques consist of prefabricated systems that do not allow for in-field installation without removal of the existing brace as the shell is pre-formed (Feng et al. 2013; 2017; 2019). There should be no difference in the behaviour of a prefabricated shell and one fabricated in-situ, provided enough overlap is present when creating the shell in the field. The main difference between the two systems being the fabrication technique used. A field fabricated system would require quality controls to ensure the final product functions as designed.

Studies completed by El-Tawil and Ekiz (2008; 2009) investigated an infield application of the FRP-BRB technique that inhibited bonding between the steel core and filler material. The main difference between their research and that which was done in this paper, is that the filler material consisted of blocks of mortar or polyvinyl chloride (PVC), rather than a continuous self-consolidating grout core. Another difference being that the system investigated for this paper makes use of a shell that is fabricated from pre-impregnated flexible sheets of FRP that double as a formwork for the filler, where as El-Tawil and Ekiz (2008; 2009) used a wet-lay-up FRP system that was applied once the filler had been secured to the core. Other studies have conducted physical tests, as well as using elastic buckling analysis and finite element modelling, to investigate filler materials such as pultruded GFRP pipes and bamboo sticks (Deng et al. 2015; Feng et al. 2017, 2019). These previous studies are of systems that have different compositions and use different construction techniques than that of the system studied in this paper.

The goal of this research is to understand the behaviour and structural capabilities of the proposed hybrid FRP-BRB strengthening system through small scale testing. It is important to ensure that the pre-impregnated flexible sheets of FRP is stiff and strong enough to act as a form for the filling grout and not to fail under hoop and axial stresses providing a secure yielding condition for the steel core. It is also essential to have design procedure to determine an optimum shell diameter and grout strength providing yielding condition for the steel core and preventing the buckling of the system. The outcome of this study will help establish a platform that will allow for reliable and optimum design procedures, applicable to strengthening slender steel members in aging infrastructure, to be developed; especially for those cases where the removal of the existing member is not an option.

EXPERIMENTAL PROGRAM

Test Matrix

A total of 27 FRP composite shells were prepared with three different lengths (300 mm, 600 mm, and 900 mm) and three different diameters. The outer diameters of the tested shells were 41 mm, 53 mm and 65 mm. Hot rolled rectangular steel bars (25.4 mm x 6.35 mm) were cut at lengths 30 mm longer than their corresponding shell lengths. Bars were prepared with 45 mm long tapered tabs on all ends. The steel was lubricated and grouted inside its corresponding shell length. It is understood that flat steel plate is not commonly used in bracing, however this study is done in order to understand the behaviour of the system as a whole. Future studies should include various cross sections. For each diameter and shell length, three identical samples were fabricated as shown in Table 1. The test samples are identified with a specimen identification (ID) of the form L*X*-D*Y*(*Z*), where *X* stands for the length of the FRP shell of 300 mm (L300), 600 mm (L600) and 900 mm (L900); *Y* stands for the size ranking of the outer diameter of the FRP shell with D1 corresponding to the smallest diameter

and D3 to the largest; and *Z* is the sample number of either 1, 2 or 3. As an example, L300-D2(2) is the specimen with a 300 mm long shell, a 53 mm outer diameter and is the 2nd of three identical samples.

Along with the 27 reinforced specimens, 9 plain steel samples were fabricated and tested. These specimens were identical to the steel cores of the reinforced specimens and three of each length were tested. Specimens are identified by the length of the FRP shell that they would have been reinforced with, as well the sample number (1, 2, or 3). For example, the second of its length plain steel specimen with overall length of 630 mm is identified as L600(2). Table 1 provides a summary of all specimens. It is noted that due to difficulty in fabricating the smallest diameter, the L600 specimens were observed to have outer diameters of 38 mm rather than 41 mm.

Material Properties

FRP Shell: FRP shells were fabricated of a pre-impregnated glass FRP laminate (PipeMedic 2019) made of bidirectional fabric in conjunction with an epoxy-based adhesive (QuakeBond 2019). Shells were constructed to have two layers of the laminate with approximately one quarter of the circumference in overlap. The material was measured to have a ply thickness of approximately 0.35 mm. Five identical coupons in both the warp (i.e. longitudinal direction of the roll of fabric) and fill (i.e. transverse direction of the roll of fabric) directions of the FRP were prepared and tested in tension. The warp direction of the fabric will be orientated to become the hoop direction on the FRP shells, leaving the fill direction to be orientated in the axial direction. Coupons consisted of 4 layers of the FRP laminate with approximately 1 mm of adhesive between layers and were prepared and tested as per ASTM D3039 (2017) and ASTM D7565 (2017). Four layers of the FRP were used, rather than the standard two, as the material was thin and fragile which made it difficult to test. In the warp direction, the test results showed an average (± standard deviation) modulus of elasticity of

17.16 ± 0.47 GPa (using longitudinal strain range 1000 – 3000 με), average rupture stress of 192.79 ± 1.54 MPa, average rupture strain of 1.33 ± 0. 04 % and a secant modulus of 14.50 ± 2.85 GPa. The secant modulus is the slope of the stress-strain curve assuming the behaviour is linear up to the rupture, calculated by dividing the rupture stress by the rupture strain. In the fill direction, the test results showed an average modulus of elasticity of 14.14 ± 0.20 GPa, average rupture stress of 141.16 ± 16.06 MPa, average rupture strain of 1.16 ± 0.17 % and a secant modulus of 12.19 ± 3.93 GPa. The failure mode of the FRP coupons was rupture for all samples. Two of the five identical coupons in the warp direction were excluded from the results as they did not fit the trend. Figure 1 shows the experimental stress-strain relationship for both the warp and fill directions of the FRP laminate. All mechanical properties were calculated based on the thickness of 0.35 mm per ply of the laminate.

Steel Core: The hot rolled steel bars used for the specimens were 1018 mild/low carbon steel. Testing of dog-bone coupons, as per ASTM A370 (2019), concluded that the steel core material had a modulus of elasticity of 194.8 GPa and a yield strength of 353 MPa. The failure mode of the steel coupons in tension was yielding.

Self Consolidating Grout: The self consolidating grout was designed to have a 28-day compressive strength of approximately 35 MPa with a high slump to allow for the grout to flow easily into the FRP shells with no vibration or consolidation required. The grout is composed of masonry sand (Shaw Resources, Milford, Halifax, NS, Canada), CRH Type N cement, Euclid Plastol 6400 superplasticizer, and water. The L300, L600, and L900 specimens were fabricated with grouts having compressive strengths of 34.7 MPa, 19.5 MPa, and 34.4 MPa, respectively. The goal was to have a grout strength of 35 MPa for all specimens and the mix was designed as such, however, due to unforeseen problems,

this was not achieved for L600 specimens. The elastic modulus of the grout samples was not measured.

Specimen Fabrication

The FRP laminate was cut to the appropriate length and width allowing for 2 layers and ¼ the circumference in overlap, where the warp direction of the roll of material was oriented in the hoop direction of the shell. The two-part adhesive was mixed manually until a uniform colour and consistency was achieved. Adhesive was then applied at a thickness of approximately 1 mm over all but one circumference in width of the sheet, as shown in Figure 2. PVC pipes of outer diameters 33.5 mm, 48.1 mm and 60.2 mm were covered in a thin layer of plastic to inhibit accidental bonding to the pipe and facilitate removal of the FRP shell once cured. The FRP was securely wrapped around the pipe and then secured with an additional plastic sheet wrapped around and fully taped to ensure the shell did not loosen during curing. After 24 hours of curing, the shells were unwrapped and removed from the PVC.

Steel cores were prepared with 45 mm long tapered tabs to avoid premature local buckling at the fixtures during testing, as shown in Figure 3. Tabs were added after early testing showed that the steel core would locally buckle outside of the shell if un-strengthened. In practical full-scale application, it is unknown if the additional strengthening would be required. It is possible that the connection of the steel core to the structure may provide additional stability. Large scale testing of the system is required to confirm. Small pieces of expanded polystyrene were glued to the steel tabs at the ends of the steel cores to limit the transfer of force into the grout during testing. The cores were then coated in a thin layer of petroleum jelly, allowing the steel to act independently of the grout and shell. A wood stand was designed to keep the steel centered within the FRP shell while casting and curing the grout. To ensure that the steel remained centered in the shell while curing, cut outs on the

top cover and bottom were aligned to restrict movement. The self consolidating grout was then funnelled into the shell until it reached the top and then the clear plastic cover was lowered onto the specimens. The alignment of the steel core and FRP tube was confirmed visually and by using a level. After a minimum of 24 hours the specimens were removed from the frame and cured in sealed plastic bags at room temperature for a minimum of 28 days. Prior to testing, both ends of each specimen were strengthened with a 75 mm width of unidirectional basalt FRP using an epoxy resin as the matrix. Two layers were applied with the fibres in the axial direction and two and a half layers were applied with fibres in the hoop direction. This ensured the test results would not be governed by bursting of the shell at the ends. After at least 7 days of curing of the end FRPs, the specimens were tested.

Instrumentation and Test Setup

As shown in Figure 4, pin-pin conditions were simulated with test fixtures that allowed for 5 mm at both ends of the steel to be loosely slotted into the test plate on either end, preventing slip out during testing while allowing rotation. The 5 mm slot was confirmed during testing to be shallow and wide enough to allow for rotation of the steel core at both ends. Before being cast into the FRP shells, two strain gauges (SG1 and SG2) were installed at mid-height on each steel core. Once the specimens were prepared and cured two more strain gauges (SG3 and SG4) were installed at mid-height on the surface of the FRP shell directly over the steel strain gauges. In addition to the strain gauges, two lateral linear potentiometers (LP1 and LP2) were set up along the longitudinal axis of the specimen to measure the extent of the lateral displacement at mid-height. In order to ensure the lateral potentiometers did not slip off during testing, and to allow the placement to be directly over the strain gauges, small aluminum plates were installed to bridge the strain gauges. The test set up is shown in Figure 5. Once specimens were fully prepared and cured, they were tested in compression using a universal testing machine. The loading rate of the machine was set to have an overall displacement

rate of 2 mm/min. Load, displacement, and strain data were collected by a data acquisition system with 10 Hz frequency for the L300 specimens and 100 Hz frequency for the L600 and L900 specimens to capture sudden buckling failure.

RESULTS AND DISCUSSIONS

Failure Modes

Two primary modes of failure were observed for the compression testing of the small-scale FRP-BRB specimens, namely: yielding of the steel core and overall buckling. The primary failure mode was not necessarily the ultimate failure mode of the specimen. For specimens that yielded first, more load was often taken by the specimen until ultimate rupture or buckling. A photo of all tested specimens is provided in Figure 6 and a summary of all test results is provided in Table 2. All but L300 D2 and D3 specimens ultimately failed by buckling of the entire system. When specimens failed ultimately in buckling, cracking of the FRP shell and grout was seen on the tension side and crushing of the shell and grout on the compression side. L300 D2 and D3 failed by FRP and grout rupture as is seen in Figure 6.

The tests were conducted successfully to evaluate the effectiveness of the shell and grout maintaining the stability of the steel core to be yielded. The system worked very well way beyond of the yielding point. For shorter specimens, as post-yielding buckling was not possible, the length of the steel core decreased to a point that the cross-beam in contact with the shell and engaged all three components of the system (i.e. steel, grout, and shell). At this point, the load begins to be applied to all three components showing an upturned tail. This will be further discussed in the next section. The upturned tail of the curves has been reported just in case the reader wanted to analyze it further. All tests were continued until a peak load in which the specimen was not able to take more load.

Peak load was taken as the ultimate failure load of each specimen, for specimens that buckled without yielding this was taken as the buckling load and for specimens that experienced yielding of the steel core it was taken as the ultimate load at rupture. The yield load was determined using two methods. The first method was by comparing the strain in the steel, recorded by the strain gauges, to the yield strain as per Hooke's law and the experimental yield stress and modulus of elasticity. The yield strain was calculated to be 0.0018 mm/mm. When compared to the steel strain, the corresponding load was taken to be the yielding load. On occasion the steel strain gauges failed prematurely due to complications with being cast in grout. These situations have been noted in the table. When the specimen buckled prior to yielding the yield strain and corresponding load was also not recorded. The second method used to calculate the yielding load was by visually locating the first peak on the load-stroke diagrams shown in Figure 7. This method was only possible for graphs that had a defined peak. Specimens that buckled very close to what was considered a yielding load were marked as inconclusive as it was not possible to determine whether buckling or yielding occurred first. The buckling load for specimens was recorded as the peak load when no obvious yielding had occurred. Using a combination of these three loads, the failure mode was described as either yielding of the steel core or buckling. Specimens where steel strain data was not available and/or visual yield peaks were inconclusive, the failure mode was marked as such.

The yielding load for all specimens ranged from 51.8 kN to 69.4 kN with an average of 62.5 kN. Based on the yield stress of the steel and cross-sectional properties, the yield load for the steel was calculated to be approximately 56.9 kN. The difference in loads is thought to be due to some of the test load being carried by the grout, likely at the top and bottom of the specimen where the steel tabs are located. The system was deemed to be successful if the system was able to reach yielding of the steel core. Systems that ultimately failed shortly after or seemingly simultaneously with the

yielding load indicate that the diameter of the system was close to optimal for that slenderness ratio of the steel core. Specimens that carried more load past that point were less efficient as failure was still decided by the yielding load.

Load-Stroke Behavior

Load and stroke were recorded during testing of all 36 specimens. Although it is understood that stroke is not a reliable form of information, the data was used to gain a general understanding of the behaviour of the FRP-BRB systems. The stroke data was not used in any calculations. The load-stroke graphs are provided in Figure 7. There are various regions that are similar in all graphs, labelled i-v on the graph for L300 as an example. The first region, i, is the linear region of the graph. Region ii is the visual yield point of the specimens; this is the first peak seen on the graph. This region does not occur in specimens that buckled prior to yielding as previously described. Region iii corresponds to the relatively flat plateau of the graph that shows increasing load with a much lower incline compared to the initial slope in region i. Region iv is the point at which the load begins to be applied to the grout and shell. This occurs around 15 to 20 mm of stroke, which is approximately the amount of free steel outside of the shell before any load is applied. The steel was compressed to the height of the shell at which point the cross-beam of the testing machine came in contact with the shell and grout and began loading the entire specimen. This occurrence was seen to happen visually during testing and is noted to be due to the test method and scale of the specimens. The final region noted, v, is the rupture point of the specimens. This region varies for each size and length specimen and is the point of ultimate failure.

For the L300 specimens, two of the D1 diameter specimens buckled or ultimately failed close to the common yielding point. These specimens were noted as having inconclusive visual yielding loads, as visually is it not possible to determine whether the specimen yielded first or buckled. The

fact that these occurred so close together leads to the conclusion that the diameter of these specimens is close to an optimal value. The optimal condition being that the load required for yielding is equal to the load required to buckle the system. As the system is consider to have failed once yielding occurs, any additional load carried past that point would be a "bonus" or safety net.

The plain steel core was also tested in compression in order to determine the buckling load corresponding to each length used in the small-scale FRP-BRB's. Three of each length were tested in compression at a rate of 2 mm/min on a 100 kN Instron 8501 Universal Testing Machine. Data was recorded at 100 Hz frequency. The test parameters were identical to the reinforced sections; however, they were tested on a smaller machine to ensure precision in the data. The average buckling loads were 21.0±2.4 kN, 5.5±0.7 kN and 1.8±0.5 kN for L300, L600 and L900 length steel, respectively.

The failure load of the FRP-BRB system is described as either the yielding load of the specimen, or the buckling load if the system was unable to reaching yielding. The ultimate or peak failure load of the specimen is the load at which the specimen was unable to carry any additional load, typically experiencing an overall system buckling and/or rupture. Table 3 presents the ratio of the average failure load and average ultimate failure load of each size specimen to the failure load of the plain steel specimens tested in compression. At a minimum, the system allowed for 2.84 times the load carrying capacity of the plain steel. As can be expected, the larger the diameter of the specimen, the larger the increase in load carrying capacity. Systems that did not sufficiently reach the yielding load of the steel core, such as L600-D1 and L900-D1, still saw an increase of 7.63 and 17.10 times the plain steel, respectively.

Load-Lateral Displacement Behavior

Two lateral potentiometers recorded the lateral displacement of the specimens as they went through the process of buckling. It is important to note that the specimens did not always buckle exactly at the

location of the gauges therefore the data may not have fully caught the extent of the buckling, but it is a good approximation. The graphs in Figure 8 shows the extent of this movement, providing the average absolute movement from the two LP's for each of the 27 specimens. The peak of each curve corresponds to the peak failure load of each specimen. It is seen that the longer the specimen, the larger the lateral displacement is at buckling or peak load. L300-D2 and L300-D3 specimens experienced little to no lateral displacement during the test. The movement that was experienced was due to rupturing and expansion of the FRP shell and grout.

Load-Strain Behavior

Strain gauges were installed at mid height on both sides of the weak axis of the steel core in order to gather compression strain data in the core prior to buckling, and both tension and compression data during buckling. Although carefully installed, complications with being cast in grout led to a few gauges failing prior to testing. It was seen with the surviving strain gauges that once the steel core yielded the strain gauges failed, likely due to being detached by the surrounding grout. This data was used to determine the yielding load that corresponded to the yield strain of the steel. Figure 9 provides the load vs strain diagrams for the steel constituent of all reinforced specimens. The average yield strain was calculated to be 1,800 με based on tensile testing of the steel. This is shown on all three graphs with a dashed vertical line. For comparison, two of each length of plain steel specimens were tested with axial strain gauges on both sides at mid height. The load vs axial steel strain diagram for these tests is provided in Figure 10 with the yielding strain marked with a dashed vertical line.

Additional strain gauges were also installed at mid height of the FRP shell parallel to the steel strain gauges, along the weak axis. These gauges recorded strain in the FRP shells during testing, recording compressive strain as well as tensile strain during buckling. This data was also used to interpolate the strain in the grout under the assumption that the FRP shell and grout were perfectly

bonded and shared the same strain data. Figure 11 provides the load vs axial shell strain diagrams for all three length specimens. Based on tensile testing of the FRP material, the rupture strain in the axial direction of the specimens was found to be 11,600 με. The peaks of each curve in Figure 11 correspond to the peak failure load of the specimen. The strain at these peaks do not exceed 11,600 με in tension. The compression failure strain for the FRP material is unknown but is assumed to be similar to the tension strain, but likely lower. Considering this assumption, Fig. ***11*** shows that the compressive axial strain of the FRP shells did not reach the crushing strain of FRP in the tested specimens. This is compatible with failure mode of the specimens pictured in Figure 6.

As much of the calculations assume that the system is linear elastic until failure, it is important that the grout remain un-cracked for this assumption to hold. The rupture strain of concrete is calculated by a combination of Equation (1) of A23.3-14 Design of Concrete Structures (CSA Group 2014) assumed to be valid for the self-consolidating grout used in this research) and Hooke's law to form Equation (2) as follows:

$$f_r = 0.6\sqrt{f_c'} \tag{1}$$

$$\varepsilon_r = \frac{f_r}{E_g} = \frac{0.6\sqrt{f_g'}}{4500\sqrt{f_g'}} = \frac{0.6}{4500} = 133\ \mu\varepsilon \tag{2}$$

where f_r is the rupture stress of normal density concrete, f'_c is the compressive strength of concrete, or grout (f'_g) in this case, ε_r is the rupture strain of concrete, and E_g is the modulus of elasticity of the grout. The modulus of elasticity of grout was calculated by the equation for the modulus of elasticity of concrete provided in A23.3-14 Design of Concrete Structures (CSA Group 2014), shown as the denominator of Equation (2), and was assumed to be valid for the grout.

Based on this equation the rupture strain for the grout is 133 με. Table 4 provides the FRP strain at the visual peak loads for every specimen. Based on Table 4 it is seen that when the grout is

in tension (positive strain values, bolded in table) this value was only exceeded when the specimen buckled prior to or very shortly after yielding, such as in all D1 sized specimens and two of the L600-D2 specimens which buckled very shortly after yielding. This implies that the assumption that the specimens are linear elastic until yielding is reasonable.

Contribution of Components to Total Load

The goal with the specimens is to load the steel core directly with little to no load being carried by the grout and FRP shell. In order to confirm if this was achieved, the strain in the steel, shell and grout were converted to load based on their individual moduli. Once these were evaluated the total calculated load was then the sum of the three components. This allowed for a comparison between the calculated total load and the load recorded by the data acquisition system. This also allowed for an estimate of proportionally how much load was carried by each component during different stages of testing. As the calculations are based on the assumption that the specimens are linear elastic, the analysis is only accurate up until yielding of the steel core. The data continues past this point; however, caution must be taken in interpreting this information. The load carried by the individual components are calculated by the general equation as follows:

$$P_i = \varepsilon_i E_i A_i \tag{3}$$

where i is either s for steel, g for grout, or f for FRP, P_i is the load, ε_i is the strain, and A is the cross-sectional area of the component i. For the steel, the strain is taken to be the absolute value of the average of the two recorded strain values as both are in compression up to yielding. For both the grout and the FRP the strain was also taken to be the absolute value of the average of the two recorded strains. This is based on the assumption of super position of the strain due to the compressive force, with the strain due to the moment as the specimens start to buckle. A sample of the graphs for this analysis was provided for one specimen of each length with diameter D2 in Figure 12. It is important

to note that this analysis was not preformed if a specimen did not have any reliable steel strain data, such as for L300D1(1) and L300D2(3).

During initial testing hoop strain in the FRP shell was recorded. It was found that very little hoop strain was present before yielding and therefore minimal confinement effects were present. Hoop strain was not recorded in further tests as only linear behaviour up to yielding was investigated.

Table 5 provides the ratio of each component to the calculated total load for all specimens. The contribution of steel to the total load ranges from 71% to 97% with an average of 87%, 94% and 77% for L300, L600 and L900 specimens, respectively. The overall average for the steel contribution is 86%. The contribution of the grout to the total load ranges from 3% to 28% with an average of 13%, 6%, and 24% for L300, L600 and L900 specimens, respectively. The overall average for grout contribution is 13.5%. The contribution of the FRP shell to the total load ranges from 0.1% to 1.3% with an average of 0.3%, 0.1% and 0.6% for L300, L600 and L900 specimens respectively. The overall average contribution for the FRP shell is 0.5%. In a perfect system, the grout and FRP would carry no load, however, it is believed that the tapered plates installed at the ends of the steel core (to inhibit local buckling) allowed for a small amount of the load to be transferred to the grout and therefore the FRP shell as well.

ANALYTICAL STUDY

A simple analytical study was conducted to predict the governing failure mode for each specimen to determine whether the failure would be by system buckling or yielding of the steel core. The model is not able to predict the load-deflection behavior of the test specimens. It represents a simple calculation to determine required flexural rigidity of the FRP-BRB system to prevent buckling of the steel core.

Description of Model

The critical flexural rigidity (EI_{crit}) of the specimens is established by equating the load required to yield the steel core (P_y) in Equation (4), to the load required to buckle the FRP-BRB system (P_{cr}), Euler's critical load equation. The result of this is presented as follows in Equation (5):

$$P_y = A_s f_y \tag{4}$$

$$EI_{crit} = \frac{A_s f_y L^2}{\pi^2} \tag{5}$$

where P_y is the yield load for the steel core, A_s is the cross-sectional area of the steel core, f_y is the yield stress of the steel core, EI_{crit} is the critical flexural rigidity, and L is the un-supported length of the steel. The equation can be modified to account for different steel core cross-sections. To determine whether the composite specimens would have a yielding failure or buckling failure, the actual flexural rigidity was computed and compared to the critical values. The combined EI is calculated by adding the EI for each component of the specimen as outlined in Equation (6). The equation for calculating the combined EI is adopted from Xie (2005) with a term added for the FRP shell as follows:

$$EI = E_s I_s + E_g I_g + E_f I_f \tag{6}$$

where E is the modulus of elasticity of either the steel core (E_s), the grout (E_g), or the FRP shell in the axial direction (E_f), and I is the moment of inertia of either the steel core (I_s), the grout (I_g), or the FRP shell (I_f). Figure 13 shows the three components considered in the analysis, the steel core (s), self-

consolidating grout (*g*) and the FRP shell (*f*). For verification of the test data, the modulus of the steel was taken as the experimental value, 194.8 GPa. The modulus of the SCG was calculated using the corresponding grout strength (f'_g) for each length specimen. The modulus of the FRP was take as the experimental value in the axial direction, 14.14 ± 0.20 GPa.

The contribution of steel (EI_s) was calculated about the weak axis. For the contribution of the grout (EI_g) it was assumed that there was no cracking in the grout. This assumption is only valid up to the yield point of the specimen, assuming buckling does not take place first. The contribution of the FRP shell (EI_f) was calculated using the experimental modulus of elasticity and the moment of inertia for a thin walled cylindrical shell. Once the EI was determined, it was compared to the critical EI to predict the mode of failure of the specimen. If the flexural rigidity of the composite member was greater than the critical flexural rigidity, it was predicted that the specimen would yield first. If the composite EI was less than the critical buckling EI, it was rendered that the specimen would buckle first. Predictions and actual failure modes for the specimen are presented in Table 6. It is important to note that this model can adequately predict if buckling would be the failure mode, however, it will not accurately predict the load associated with the buckling failure as it is no longer linear elastic and the extent of the grout cracking is unknown. This is not an issue for practical design as the goal of the FRP-BRB system is to achieve yielding as the first mode of failure, and therefore, the systems will be designed and sized to achieve the goal.

Using the model, it is also possible to determine the optimal diameter for the various configurations and lengths of FRP-BRB systems. The optimal diameter is simply defined as the diameter of the FRP shell that would allow the steel core to yield and the system to buckle simultaneously. This is done by setting the critical buckling flexural rigidity equal to the total flexural rigidity and solving for the diameter of system that satisfies the equation shown in Equation (7).

$$EI_{crit} = E_s\left(\frac{bh^3}{12}\right) + 0.25E_g\left(\pi\left(\frac{D_g}{2}\right)^4 - \frac{bh^3}{3}\right) + 0.25\pi E_f\left(\left(\frac{OD_{optimal}}{2}\right)^4 - \left(\frac{OD_{optimal} - t_f}{2}\right)^4\right) \quad (7)$$

where E is the modulus of elasticity of either the steel core (E_s), the grout (E_g), or the FRP shell (E_f), b is the base dimension of the steel core, h is the height dimension of the steel core, D_g is the diameter of grout, equal to the outer diameter of the FRP shell, less the thickness of the FRP shell and adhesive, $OD_{optimal}$ is the optimal outer diameter of the FRP shell, and t_f is the thickness of the FRP shell, excluding the adhesive. It should be noted that the equation is only applicable for rectangular steel core sections and assumes the core is centered in the shell and is loaded along this line. This equation must be modified before being applied to other cross-sections of steel. This calculation of the optimal diameter does not account for safety requirements. A reliability analysis is recommended for establishing a strength reduction factor or factor of safety for the system.

Parametric Study

Effect of Grout Strength: The grout provides lateral support to the steel core in order to help inhibit buckling. The quality of grout and its relationship to the performance of the system was investigated. In order to do so, the flexural rigidities of the three FRP shell diameters, 41 mm, 53 mm, and 65 mm, were calculated for grouts varying from 10 MPa to 50 MPa. Although the factor that directly impacts the behaviour of the system is the modulus of elasticity of the grout, strength of the grout was investigated as it is a more common attribute in practice. These flexural rigidities are represented as "X"'s in Figure 14. In order to compare these values directly, two FRP layers were assumed for all specimens and the steel core was the same flat plate, 25.4 mm x 6.35 mm, as used in the experimental studies. Noted on the same figure are the critical buckling flexural rigidities for the three lengths investigated, L300, L600 and L900. These horizontal lines allow for the failure mode to be predicted for each diameter and grout strength. If the "X", or flexural rigidity, for a system falls above a critical

line it implies that for a specimen at that length, the composite EI is larger than the critical EI and therefore the system (at that length) would experience yielding of the steel core. If the "X" falls below the line, it implies the opposite and a buckling failure is predicted at that length. For example, for an FRP-BRB system with a grout strength of 30 MPa, diameter D1, and length L900, the system is predicted to buckle as the "X" falls below the line. This same specimen, at length 300 is predicted to yield as the "X" falls above the L300 critical buckling line. It is seen that the smaller the diameter of the system, the smaller the impact of increasing the grout strength is. From 10 MPa to 50 MPa grout a 90%, 106% and 110% increase in flexural rigidity is seen for D1, D2, and D3, respectively. For the smaller diameter specimens, this increase is more critical for the lengths investigated as it can switch the failure mode from buckling to yielding. This same increase in grout strength is less important for the larger diameter specimens as they succeed with even the lower grout strength and therefore any increase in strength after that is un-necessary.

Effect of Number of FRP Layers: In a similar technique to the changing grout strength, the impact of increasing the number of FRP layers on a system was explored. The grout strength was held constant at 35 MPa with the same cross section of steel used in the experimental study, 25 mm x 6.35 mm flat plate. Flexural rigidities for the three diameters, D1, D2, and D3 were calculated for one to five layers of FRP shell. These flexural rigidities are noted with "X"'s in Figure 14 and the critical flexural rigidities are denoted with horizontal lines for each length specimen. As previously explained, if the specific "X" falls above a certain critical EI line, it means that at that length, the steel core would yield at that length. If the "X" falls below the line the system would buckle at that length. The increase in number of FRP layers is seen to have an even smaller impact on the overall flexural rigidity compared to changing the grout strength. The largest impact is seen on the smallest diameter FRP shell. When changing the number of layers from one to five, an increase of 27%, 15% and 12% is

observed for D1, D2, and D3, respectively. This increase only has an impact on D1 with respect to the L600 critical buckling line. From this study we can conclude that the number of FRP layers does not have a significant impact on the flexural rigidity of the system and therefore the number of FRP shell layers should be chosen for convenience and ease of installation. The larger the diameter of the FRP it is likely additional layers will be required for added stiffness as the FRP shell acts as formwork for the self-consolidating grout.

Effect of Slenderness Ratio on Optimal Diameter: The optimal (outer) diameter for an FRP-BRB system allows for the system to buckle at the same time as the core yields. It is important to note that while this is referred to as the optimal diameter, it does not include a safety factor that would be suggested for design of the system. In other words, the optimal diameter is the minimum allowable diameter for the design of the system. Figure 15 explores the effect of changing the grout strength and slenderness ratio on the optimal diameter. The graph is designed for the small-scale specimens containing the same steel core as the experimental program assuming two layers of FRP shell. It is important to consider that when reading the optimal diameter off Figure 15, it does not account for any space between the shell and the steel core. This means that it is important to compare the suggested size for the optimal diameter, to the dimensions of the steel core and increase the diameter if needed. The point at which all lines converge around the optimal diameter of 15 mm and a slenderness ratio of approximately 70 is the point at which the system is no longer needed as the steel core alone would yield prior to buckling, eliminating the need for the FRP-BRB system. As can be expected, as the slenderness ratio of the system increases, the optimal diameter also increases. Lower strength grout requires a slightly larger diameter system, but not significantly. For example, at a slenderness ratio of 300, a system containing 10 MPa grout requires an outer diameter of 41.7 mm and a system containing 50 MPa grout requires an outer diameter of 35.3 mm. For the case of the 50

MPa grout, it is likely that due to the maximum dimension of the steel core, 25.4 mm, and the need for a safe amount of cover between the core and the edge of the grout, that the optimal diameter would be too small. This enforces the idea that a high strength grout is unnecessary for the success of the system.

Effect of Steel Core Shape: As not all braces are flat plate steel, it is important to consider more common cross-sections for the steel core. The following parametric study considers various sized angle braces at different slenderness ratios. In order of increasing size, the angles considered were 50 mm x 50 mm, 75 mm x 75 mm, 100 mm x 100 mm and 125 mm x 125 mm, all with 6 mm thick legs. For this study the grout strength was set to be 35 MPa and two layers of FRP shell were considered. The resulting graph is shown in Figure 15. For this study, it was assumed that the centroid of the angle is in line with the center of the system and that the entire system is loaded along this common centroid. The point at which all lines converge around the slenderness ratio of approximately 75 is the point at which the system is no longer needed as the steel core alone would yield prior to buckling, eliminating the need for the FRP-BRB system. Figure 15 shows that as the size of the angle section increases, and as the slenderness ratio increases, the optimal diameter increases as well. Once again, it is important to note that the optimal diameter does not account for any cover between the shell and the steel core, nor does it recognize when the diameter is smaller than the steel core itself.

FUTURE STUDIES

In this study, the performance of the proposed hybrid FRP-BRB system using small-scale specimens applying to flat steel plates under monotonic loading was evaluated. future studies should include large-scale tests using practical steel cross-sections including angles and channels for real-life bracings. in addition, cyclic loading should be considered to evaluate the hysteretic energy dissipation capacity of the system. finite element molding is also recommended to obtain more in-depth

understanding of the behavior of the system, especially considering the possible local buckling and yielding of the steel core at the ends locating out of the FRP shell and grout and proposing possible strengthening system preventing any premature failure at the ends.

CONCLUSIONS

The objective of this study was to understand the behaviour and structural capabilities of the proposed hybrid FRP-BRB system and confirm its real-life feasibility as an in-field rehabilitation technique for slender steel members. In order to achieve the objective, an experimental program consisting of 27 strengthened and 9 un-strengthened small-scale specimens were prepared and tested under uniaxial compression. Specimens were fabricated using flat plate steel cores wrapped with an FRP shell and infilled with a self-consolidating grout. A simple linear-elastic model was created in order to predict the failure mode of the test specimens, but also to create a simple design procedure for the FRP-BRB system. This model was used to analyse a variety of parameters and their effects on the behaviour of the system. The following conclusions can be drawn from this study:

- The hybrid system, when sized correctly, provided adequate lateral support allowing the failure mode to change from a sudden buckling failure to a ductile yielding failure of the steel core.
- On average, at the yielding point the steel core carries 86% of the load with the grout and FRP carrying only 13.5% and 0.5%, respectively.
- It is seen that the smaller the diameter of the system, the smaller the impact of increasing the grout strength is. From 10 MPa to 50 MPa grout a 90%, 106% and 110% increase in flexural rigidity is seen for D1, D2 and D3, respectively.
- When changing the number of layers of FRP from one to five, an increase of 27%, 15% and 12% is observed for D1, D2, and D3, respectively. This implies that the number of layers is relatively insignificant to the over all flexural rigidity of the system, particularly with a larger diameter.

- The linear-elastic model was successful in predicting the failure mode of all small-scale strengthened specimens.
- Large-scale tests should be conducted to verify the conclusions drawn from small-scale tests. Also, a reliability analysis should be conducted to propose safety requirements for design codes.

DATA AVAILABILITY STATEMENT

Some or all data, models, or code generated or used during the study are available from the corresponding author by request.

ACKNOWLEDGEMENTS

The author acknowledges the financial support of Dalhousie University, the Nova Scotia Graduate Scholarship (NSGS) and the National Sciences and Engineering Research Council of Canada (NSERC). This project would not have been possible with out the help of lab technicians, Blair Nickerson, Brian Kennedy, Jesse Keane and Jordan Maerz of Dalhousie University. The author also acknowledges QuakeWrap Inc. (Tucson, AZ, USA) for providing GFRP laminate and adhesive for the experimental program.

REFERENCES

Almeida, A., Ferreira, R., Proença, J. M., and Gago, A. S. 2017. "Seismic retrofit of RC building structures with buckling restrained braces." *Eng. Struct.,* 130, 14–22. https://doi.org/10.1016/j.engstruct.2016.09.036.

ASCE. 2016. *2017 Infrastructure report card. ASCE News*. https://doi.org/10.1017/CBO9781107415324.004

ASTM. 2017. *D7565/D7565M - Standard test method for determining tensile properties of fiber reinforced polymer matrix composites used for strengthening of civil structures.* ASTM International, West Conshohocken, PA, USA.

ASTM. 2017. *D3039/D3039M - Standard test method for tensile properties of polymer matrix composite materials.* ASTM International, West Conshohocken, PA, USA.

ASTM. 2019. *A370-19e1 - Standard test methods and definitions for mechanical testing of steel products*. ASTM International, West Conshohocken, PA, USA.

Black, C. J., Makris, N., and Aiken, I. D. 2004. "Component testing, seismic evaluation and characterization of buckling-restrained braces." *J. Struct. Eng*., 1306, 880–894. https://doi.org/10.1061/(ASCE)0733-9445(2004)130:6(880)

Carden, L. P., Itani, A. M., and Buckle, I. G. 2004. "Seismic performance of steel girder bridges with ductile cross frames using buckling-restrained braces." *J. Struct. Eng*., 1323, 338–345. https://doi.org/10.1061/(ASCE)0733-9445(2006)132:3(338)

CSA Group. 2014. A23.3-14 *Design of concrete structures.* CSA Group, Toronto, ON, Canada: CSA

CSCE. 2016. *Canadian infrastructure report card: informing the future*. Toronto, ON, Canada: CSCE

Deng, K., Pan, P., Nie, X., Xu, X., Feng, P., and Ye, L. 2015. "Study of GFRP steel buckling restraint braces." *J. Compos. Constr*., 196, 1–8. https://doi.org/ 10.1061/(ASCE)CC.1943-5614.0000567

Ehsani, M. R. 2017. "Buckling reinforcement for structural members." *United States Pat. No. US 9,719,255 B1*, USA.

Ekiz, E., and El-Tawil, S. 2008. "Restraining steel brace buckling using a carbon fiber-reinforced polymer composite system: experiments and computational simulation." *J. Compos. Constr*., 125, 562–569. https://doi.org/ 10.1061/(ASCE)1090-0268(2008)12:5(562)

El-Tawil, S., and Ekiz, E. 2009. “Inhibiting steel brace buckling using carbon fiber-reinforced polymers: large-scale tests.” *J. Struct. Eng.*, 135, 530–538. https://doi.org/ 10.1061/(ASCE)1090-0268(2008)12:5(562)

Feng, P., Hu, L., Zhang, Y., and Ye, L. 2019. “Behavior analysis of FRP tube/filling strengthened steel members under axial compression.” *Thin-Walled Struct.*, Elsevier Ltd, 134April 2018, 475–490. https://doi.org/10.1016/j.tws.2018.10.015

Feng, P., Zhang, Y., Bai, Y., and Ye, L. 2013. “Strengthening of Steel Members in Compression by Mortar-Filled FRP Tubes.” *Thin-Walled Structures*, 64, 1–12. http://dx.doi.org/10.1016/j.tws.2012.11.001

Feng, P., Zhang, Y., Hu, L., and Gong, D. 2017. “Buckling of piecewise member composed of steel and high-strength materials in axial compression.” *Thin-Walled Struct.*, Elsevier, 110October 2016, 62–74. http://dx.doi.org/10.1016/j.tws.2016.10.008

Gao, X. Y., Balendra, T., and Koh, C. G. 2013. “Buckling strength of slender circular tubular Steel braces strengthened by CFRP.” *Eng. Struct.*, 46, 547–556. https://doi.org/ 10.1016/j.engstruct.2012.08.010

Han, L. H., Tao, Z., Liao, F. Y., and Xu, Y. 2010. “Tests on cyclic performance of FRP-concrete-steel double-skin tubular columns.” *Thin-Walled Struct.*, 486, 430–439. https://doi.org/ 10.1016/j.tws.2010.01.007

Harries, K. A., Peck, A. J., and Abraham, E. J. 2009. “Enhancing stability of structural steel sections using FRP.” *Thin-Walled Struct.*, 4710, 1092–1101. https://doi.org/ 10.1016/j.tws.2008.10.007

Kersting, R. A., Fahnestock, L. A., and López, W. A. 2015. *Seismic design of steel buckling-restrained braced frames a guide for practicing engineers about the review panel. NEHRP Seism. Desi. Tech. Br.*

Kim, S. H., and Choi, S. M. 2015. "Compressive behavior of H-shaped brace strengthened with non-welded cold-formed element." *J. Constr. Steel Res.,* 112, 30–39. https://doi.org/10.1016/j.jcsr.2015.04.012

Liu, X., Nanni, A., and Silva, P. F. 2005. "Rehabilitation of compression steel members using FRP pipes filled with non-expansive and expansive light-weight concrete." *Adv. Struct. Eng.,* 82, 129–142. https://doi.org/ 10.1260/1369433054038029

PipeMedic 2019. Product Data Sheet: PipeMedic PG16.15 for Structural Strengthening and Leak Proofing. QuakeWrap Inc., Tucson, AZ, USA.

Porter, M. E., and Lopez-Claros, A. 2006. *The global competitiveness report 2006*. World Economic Forum. https://doi.org/ 10.5860/choice.44-5759

QuakeBond 2019. Product Data Sheet: QuakeBond TM J201TC Tack Coat. QuakeWrap Inc., Tucson, AZ, USA.

Sadeghian, P., Shekari, A. H., and Mousavi, F. 2009. "Stress and strain behavior of slender concrete columns retrofitted with CFRP composites." *J. Reinf. Plast. Compos.,* 2819, 2387–2396. https://doi.org/ 10.1177/0731684408092396

Schulze, E. 2016. "Germany has a crumbling infrastructure problem." *CNBC,* September 14, 2016.

Schwab, K. 2018. *The global competitiveness report 2018*. World Economic Forum. https://doi.org/ ISBN-13: 978-92-95044-73-9

Shaat, A., and Fam, A. Z. 2009. "Slender steel columns strengthened using high-modulus CFRP plates for buckling control*." J. Compos. Constr.,* 131, 2–12. https://doi.org/ 10.1061/(ASCE)1090-0268(2009)13:1(2)

Tondo, L. 2018. "Italy's crumbling infrastructure under scrutiny after bridge collapse." *Guardian,* August 17, 2018.

Tremblay, R., Bolduc, P., Neville, R., and DeVall, R. 2006. “Seismic testing and performance of buckling-restrained bracing systems.” *Can. J. Civ. Eng.*, 332, 183–198. https://doi.org/ 10.1139/l05-103

Vild, M., and Bajer, M. 2017. “Strengthening under load: numerical study of flexural buckling of columns.” *Procedia Eng.*, The Authors, 190, 118–125. https://doi.org/ 10.1016/j.proeng.2017.05.316

Wu, Z., and Grondin, G. Y. 2002. “Behaviour of steel columns reinforced with welded steel plates.” 214. 03190110

Xie, Q. 2005. “State of the art of buckling-restrained braces in asia.” *J. Constr. Steel Res.*, 616, 727–748. https://doi.org/ 10.1016/j.jcsr.2004.11.005

Table 1. Test matrix

Specimen ID	Steel Core Length (mm)	Slenderness Ratio of Steel Core	FRP Shell Length (mm)	FRP Shell Outer Diameter (mm)	FRP Shell Inner Diameter (mm)	Number of Specimens
L300	330	180	N/A	N/A	N/A	3
L300-D1	330		300	41.0	34.5	3
L300-D2				53.0	49.0	3
L300-D3				65.0	61.0	3
L600	630	343	N/A	N/A	N/A	3
L600-D1	630		600	38.0	34.5	3
L600-D2				53.0	49.0	3
L600-D3				65.0	61.0	3
L900	930	507	N/A	N/A	N/A	3
L900-D1	930		900	41.0	34.5	3
L900-D2				53.0	49.0	3
L900-D3				65.0	61.0	3
					Total	36

Table 2. Summary of test results

Specimen ID			Peak Load (kN)	Avg. (kN)	Std. Dev. (kN)	Yield Load by Yield Strain (kN)	Avg. (kN)	Std. Dev. (kN)	Visual Yield Load (kN)	Avg. (kN)	Std. Dev. (kN)	Buckling Load (kN)	Avg. (kN)	Std. Dev. (kN)	Failure Mode	Predicted Failure Mode	f'_g (MPa)
L300	Plain Steel	1	19.0	21.0	2.40	-	-	-	-	-	-	19.0	21.0	2.40	B	B	N/A
		2	19.6			-			-			19.6			B		
		3	24.3			-			-			24.3			B		
	D1	1	89.9	68.8	14.89	DNR *	51.8	1.09	60.7	60.7	0.00	-	58.3	0.32	Y	Y	34.7
		2	58.0			50.7			**			58.0			Y/B		
		3	58.6			52.9			**			58.6			Y/B		
	D2	1	154.7	153.1	2.85	DNR	58.4	0.00	58.4	59.7	2.06	-	-	-	Y	Y	
		2	155.4			58.4			62.6			-			Y		
		3	149.0			DNR *			58.1			-			Y		
	D3	1	205.7	202.0	10.94	62.2	59.0	2.82	62.3	63.6	0.87	-	-	-	Y	Y	
		2	213.1			59.4			64.1			-			Y		
		3	187.1			55.3			64.3			-			Y		
L600	Plain Steel	1	5.1	5.5	0.65	-	-	-	-	-	-	5.1	5.5	0.65	B	B	N/A
		2	6.4			-			-			6.4			B		
		3	4.9			-			-			4.9			B		
	D1 ***	1	52.5	41.9	9.41	DNR	-	-	**	-	-	52.5	41.9	9.41	Y/B	B	19.5
		2	29.7			DNR			-			29.7			B		
		3	43.6			DNR			-			43.6			B		
	D2	1	65.7	77.1	9.21	60.2	59.5	0.53	**	65.8	2.86	65.7	65.7	0.00	Y/B	Y	
		2	77.1			59.4			68.6			-			Y		
		3	88.3			59.0			62.9			-			Y		
	D3	1	137.8	136.8	5.35	58.7	59.2	1.00	71.6	67.9	4.18	-	-	-	Y	Y	
		2	129.8			58.3			62.1			-			Y		
		3	142.8			60.6			69.9			-			Y		
900	Plain Steel	1	1.1	1.8	0.52	-	-	-	-	-	-	1.1	1.8	0.52	B	B	N/A
		2	2.0			-			-			2.0			B		
		3	2.3			-			-			2.3			B		
	D1	1	27.1	30.8	3.52	DNR	-	-	-	-	-	27.1	30.8	3.52	B	B	34.4
		2	35.5			DNR			-			35.5			B		
		3	29.7			DNR			-			29.7			B		
	D2	1	78.9	76.6	4.79	72.4	69.4	2.10	64.1	65.2	2.13	-	-	-	Y	Y	
		2	80.9			68.1			68.2			-			Y		
		3	69.9			67.8			63.3			-			Y		
	D3	1	99.6	114.9	19.71	69.3	67.9	1.35	64.9	66.8	1.46	-	-	-	Y	Y	
		2	142.7			DNR *			68.5			-			Y		
		3	102.3			66.6			66.9			-			Y		

Note: DNR Data not recorded
B Buckling Failure
Y Yielding Failure
* Axial steel strain gauge failure
** Inconclusive visual yielding load.
*** L600-D1 specimen diameters were approximately 38 mm

Table 3. Summary of average strength increase due to FRP-BRB system

Specimen ID		Y or B Load / Steel Failure Load	Ultimate Failure Load / Steel Failure Load
L300	D1	2.9	3.3
	D2	2.8	7.3
	D3	3.0	9.62
L600	D1	7.6	7.6
	D2	12.0	14.0
	D3	12.3	24.9
L900	D1	17.1	17.1
	D2	36.2	42.6
	D3	37.1	63.8

Note: Y or B: Yielding or Buckling Load
Values are average of that specimen group

Table 4. Summary of strain in grout at 1st peak

Specimen ID			Grout Strain at 1st peak	
			Compression (με)	Tension (με)
L300	D1	1	-242	18
		2	-3177	2653
		3	-6953	2026
	D2	1	-115	DNR
		2	-144	-127
		3	-88	-62
	D3	1	-93	-80
		2	-100	-33
		3	DNR	5
L600	D1	1	-6005	13149
		2	-3315	5347
		3	-2092	1262
	D2	1	-794	1533
		2	-630	329
		3	-189	-49
	D3	1	-163	39
		2	-86	24
		3	-206	64
L900	D1	1	-802	381
		2	-3036	6820
		3	-1141	424
	D2	1	-356	-211
		2	-490	-54
		3	-543	-147
	D3	1	-288	DNR
		2	-244	-179
		3	-274	-93

Note: DNR: Data not recorded

Table 5. Summary of ratios of calculated load contributions to total load

Specimen ID			P_s/P_t	P_g/P_t	P_f/P_t
L300	D1	1*	N/A	N/A	N/A
		2	0.83	0.16	0.008
		3	0.76	0.23	0.012
	Average		**0.80**	**0.19**	**0.010**
	D2	1	0.91	0.09	0.003
		2***	0.90	0.10	0.004
		3*	N/A	N/A	N/A
	Average		**0.90**	**0.09**	**0.004**
	D3	1	0.90	0.10	0.003
		2	0.88	0.12	0.003
		3	0.88	0.11	0.003
	Average		**0.89**	**0.11**	**0.003**
L300 Average			**0.87**	**0.13**	**0.005**
Standard Deviation			**0.05**	**0.05**	**0.003**
L600	D1**	1	0.93	0.06	0.005
		2	0.92	0.08	0.005
		3	0.94	0.06	0.004
	Average		**0.93**	**0.06**	**0.005**
	D2	1	0.94	0.05	0.002
		2	0.92	0.08	0.004
		3	0.93	0.07	0.003
	Average		**0.93**	**0.07**	**0.003**
	D3	1***	0.95	0.05	0.001
		2	0.97	0.03	0.001
		3	0.94	0.06	0.002
	Average		**0.95**	**0.05**	**0.001**
L600 Average			**0.94**	**0.06**	**0.003**
Standard Deviation			**0.02**	**0.02**	**0.002**
L900	D1	1	0.80	0.19	0.009
		2	0.82	0.18	0.009
		3	0.73	0.26	0.013
	Average		**0.78**	**0.21**	**0.010**
	D2	1	0.79	0.20	0.007
		2	0.81	0.18	0.006
		3	0.75	0.24	0.008
	Average		**0.79**	**0.21**	**0.007**
	D3	1***	0.71	0.28	0.008
		2	0.76	0.23	0.006
		3	0.80	0.20	0.005
	Average		**0.76**	**0.24**	**0.006**
L900 Average			**0.77**	**0.22**	**0.008**
Standard Deviation			**0.04**	**0.03**	**0.002**

Note: * Axial steel strain gauge failure
** L600-D1 specimen diameters were approximately 38 mm
*** Based on only one set of FRP strain data
N/A Not available

Table 6. Predicted and actual failure modes of specimens

Shell Length	f'_g (MPa)	Outer Diameter					
		D1 (41 mm)		D2 (53 mm)		D3 (65 mm)	
		Predicted	Actual	Predicted	Actual	Predicted	Actual
300 mm	34.7	Y	Y	Y	Y	Y	Y
600 mm*	19.5	B	B	Y	Y	Y	Y
900 mm	34.4	B	B	Y	Y	Y	Y

Note: Y: Yield; and B: Buckle.
* L600-D1 specimens had 38 mm outer diameter

List of Figures

Fig. 10. Load – strain diagram for steel compression tests. Note: two identical specimens tested for each length.

Fig. 11. Load vs axial shell strain diagrams: (a) L300; (b) L600; and (c) L900. Note: three identical specimens tested for each length and diameter.

Fig. 12. Sample graphs of contribution of components to load analysis for: (a) L300-D2(2); (b) L600-D2(3); and (c) L900-D2(2).

Fig. 13. Cross-section of FRP-BRB specimens for analysis.

Fig. 14. Parametric study on variation of flexural rigidity of test specimens by changing: (a) grout strength; and (b) number of FRP layers.

Fig. 15. Parametric study on the effect of slenderness ratio on optimal outer diameter of hybrid system by changing: (a) grout strength; and (b) angle steel core size.

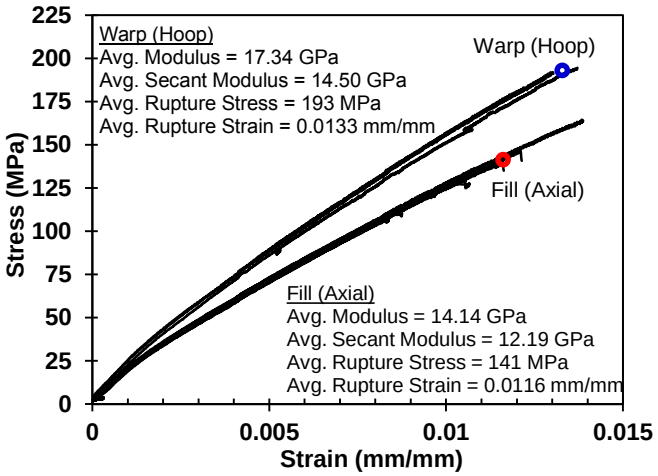

Fig. 1. FRP laminate stress-strain curves in the fill and warp directions (Note: nominal thickness of 0.35 mm per ply was used. The circles noted on each curve mark the average rupture point).

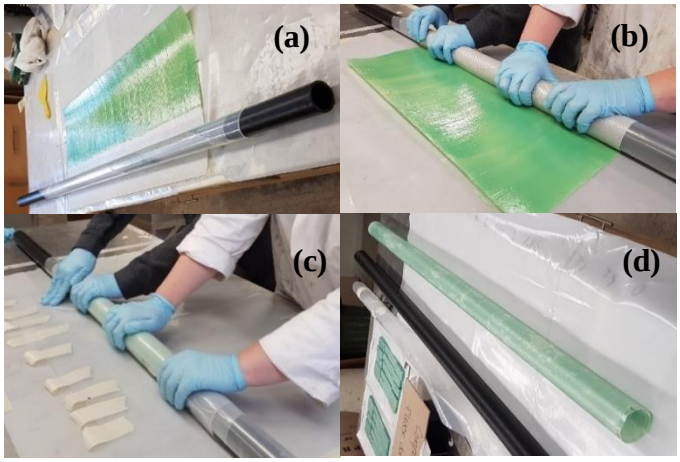

Fig. 2. FRP shell fabrication: (a) FRP sheet cut to size, two-part adhesive mixed and applied in 1 mm layer; (b) shell is wrapped around PVC tube; (c) plastic layer is wrapped around shell and entire length of shell is taped; and (d) once shell is cured, shell is removed from PVC tube and unwrapped.

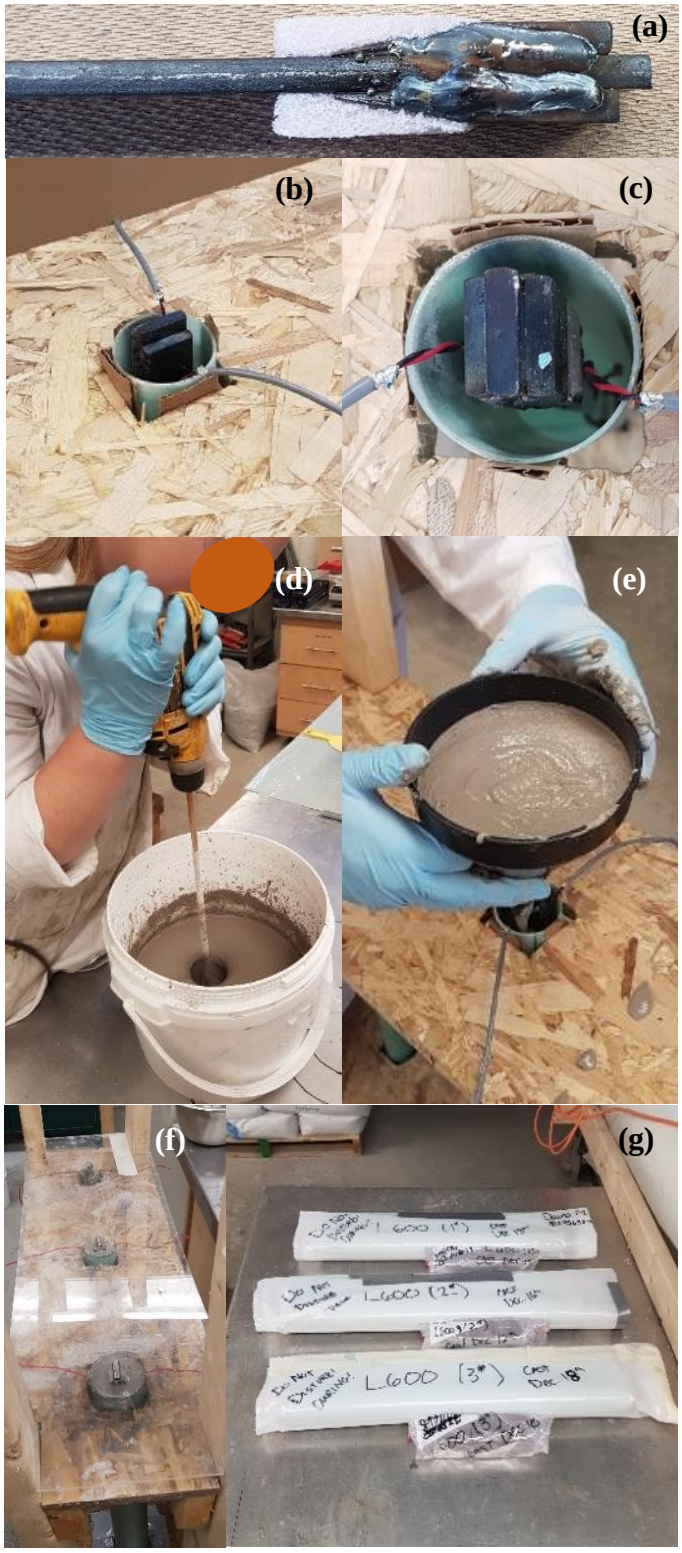

Fig. 3. Specimen fabrication: (a) steel core is prepped with tabs and expanded polystyrene (b) and (c) tube is shimmed to ensure steel core and FRP tube are aligned; (d) self-consolidating grout is mixed; (e) grout is funneled into FRP tube; (f) fiberglass cover is placed; (g) specimens cured in plastic bags at room temperature.

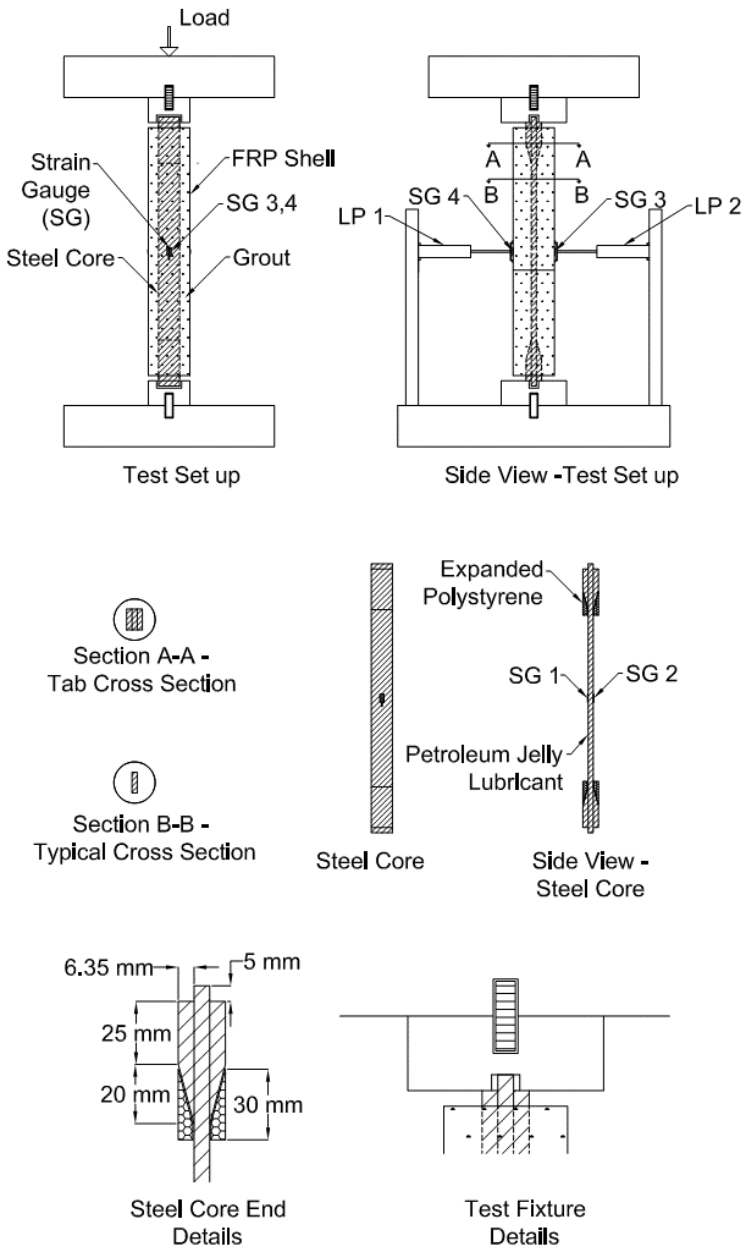

Fig. 4. Details of specimen geometry and instrumentation.

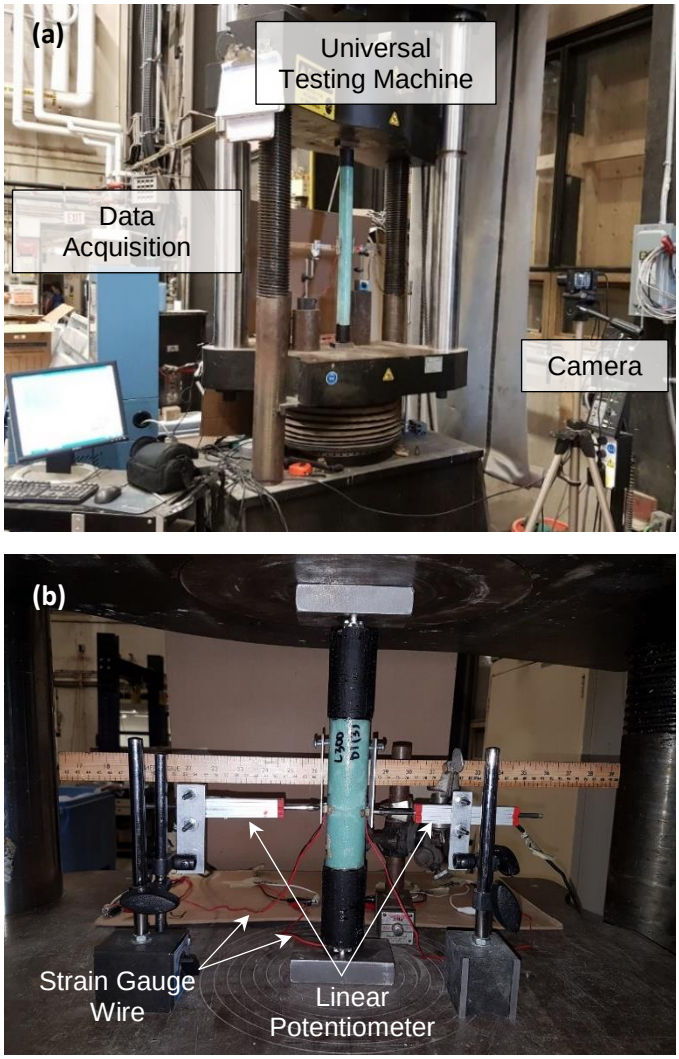

Fig.5. Test set-up: (a) overview and (b) close up of set-up of Specimen L300 D1 showing external instrumentation.

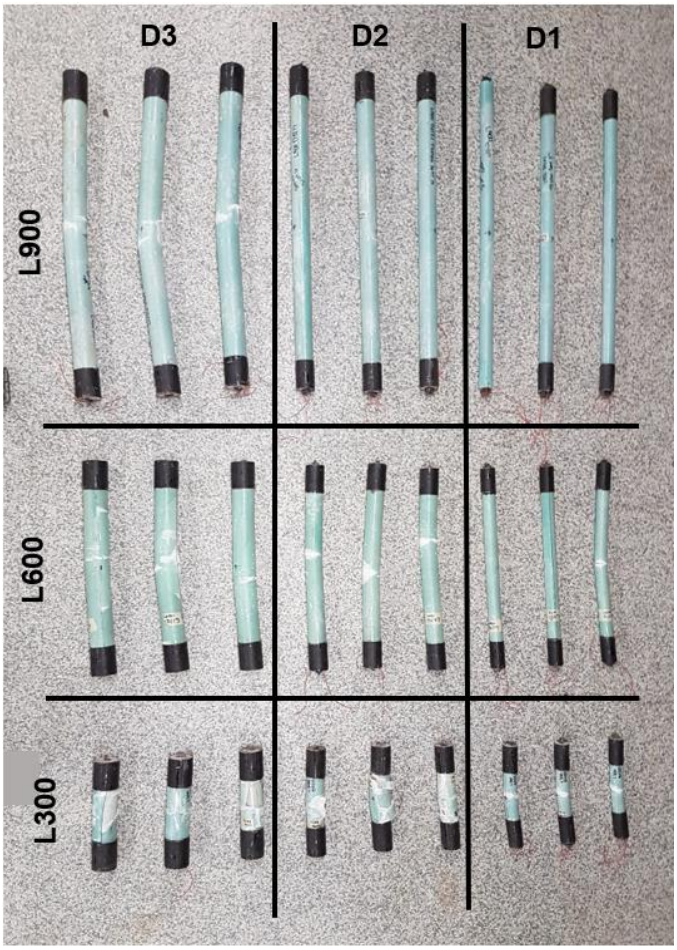

Fig. 6. Photo of all tested specimens after failure.

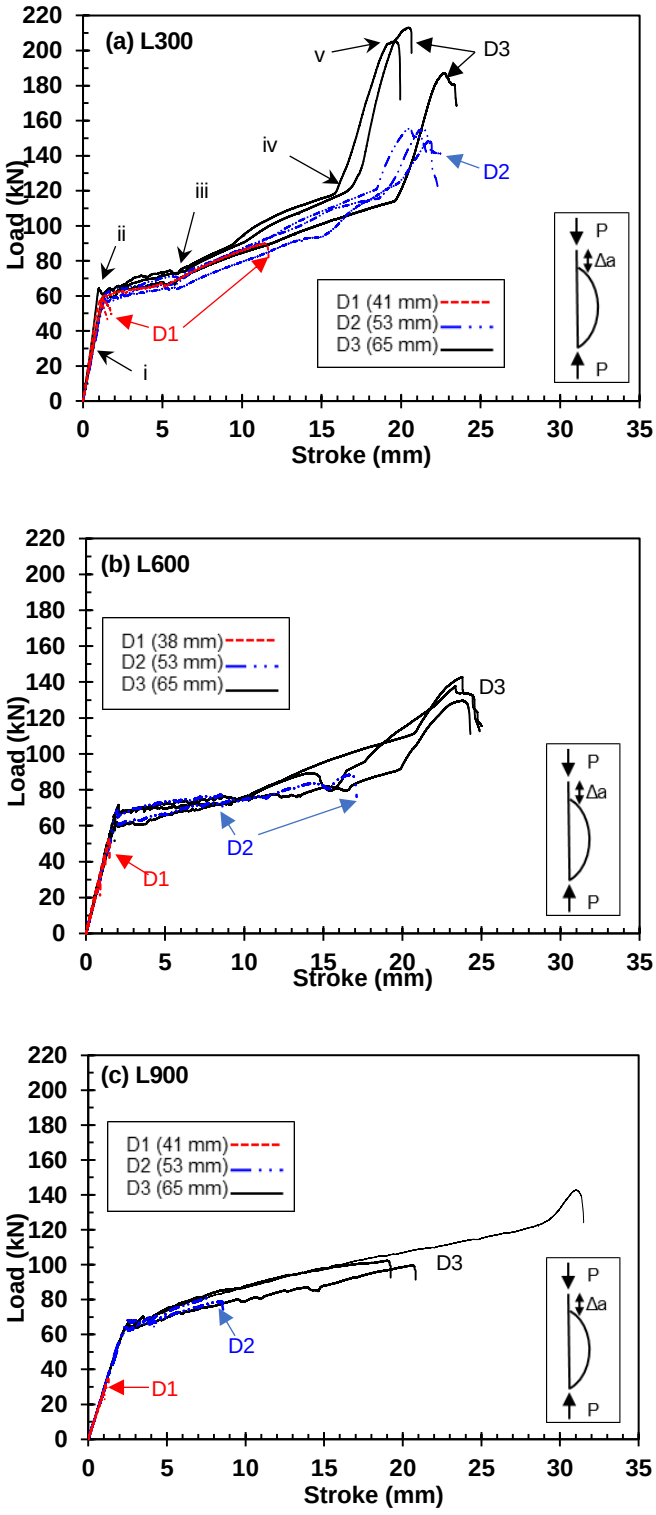

Fig. 7. Load – stroke diagrams for: (a) L300; (b) L600; and (c) L900. Note: three identical specimens tested for each length and diameter.

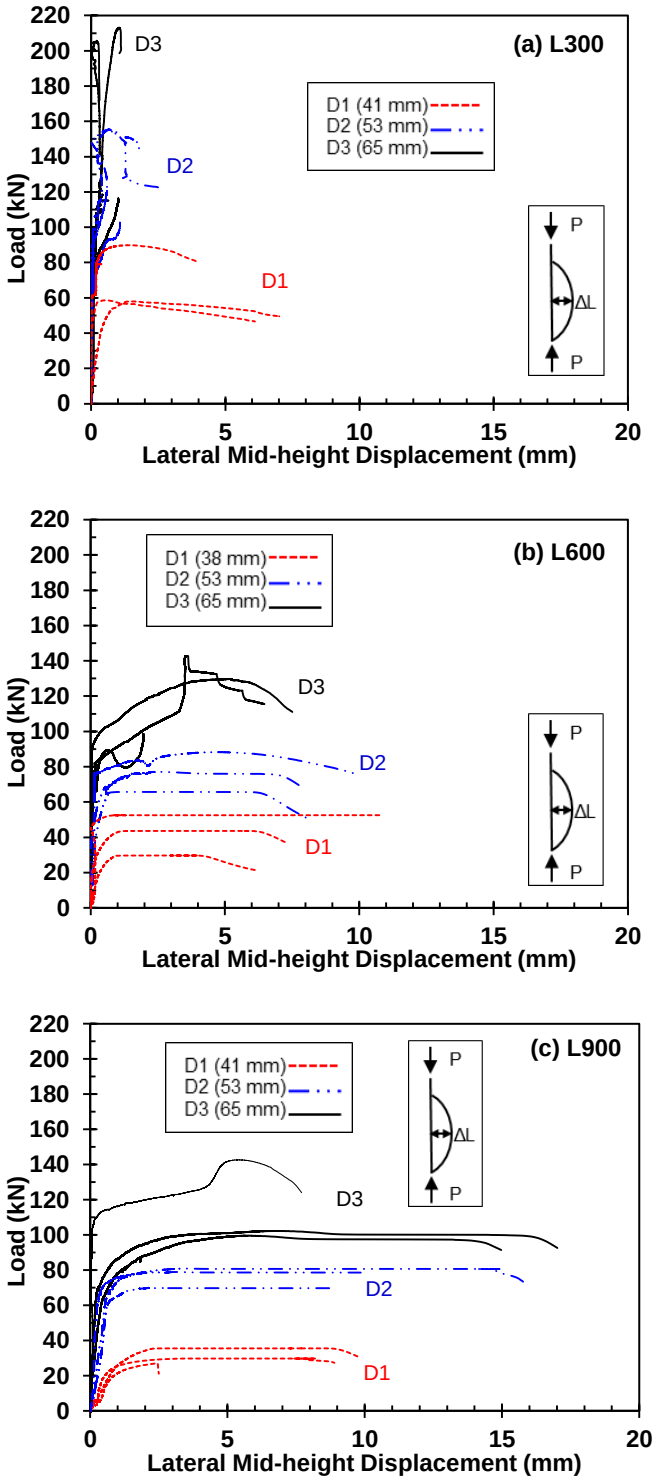

Fig. 8. Load – lateral mid-height displacement diagrams: (a) L300; (b) L600; and (c) L900. Note: three identical specimens tested for each length and diameter.

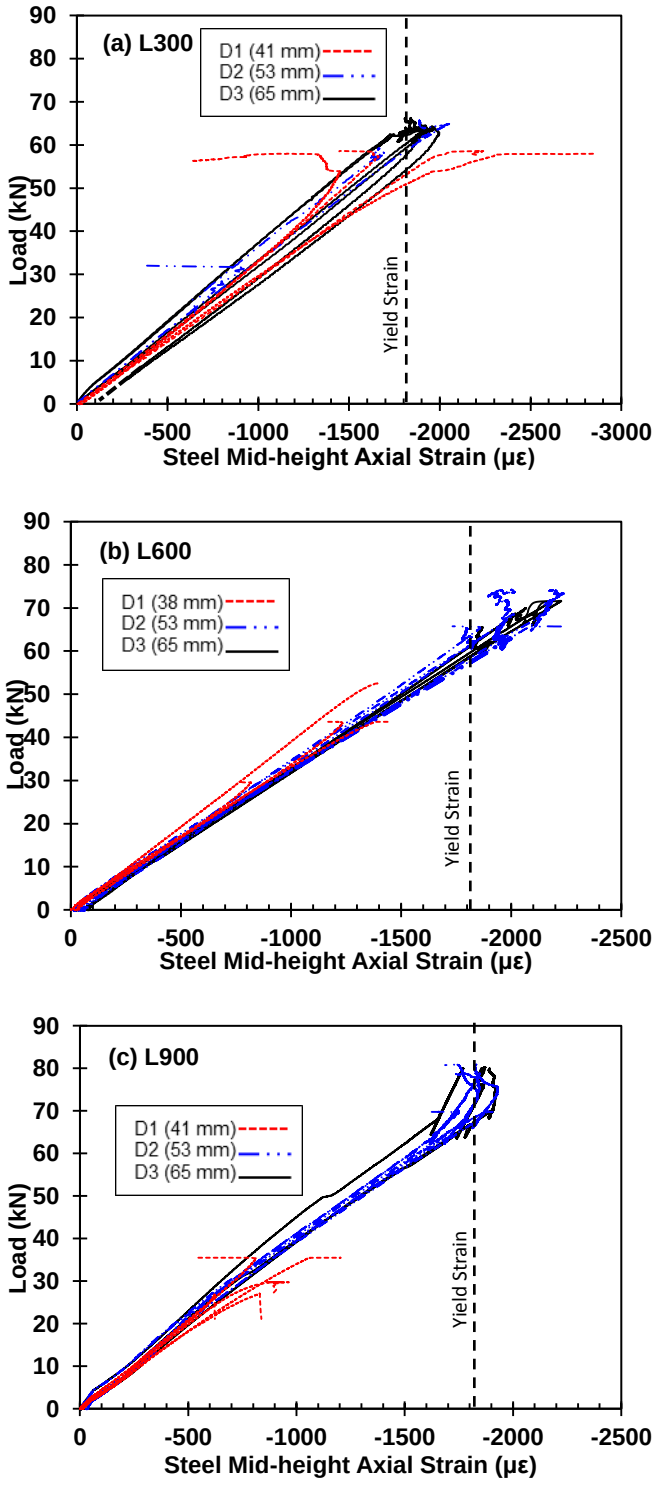

Fig. 9. Load – axial steel strain diagrams: (a) L300; (b) L600; and (c) L900. Note: three identical specimens tested for each length and diameter.

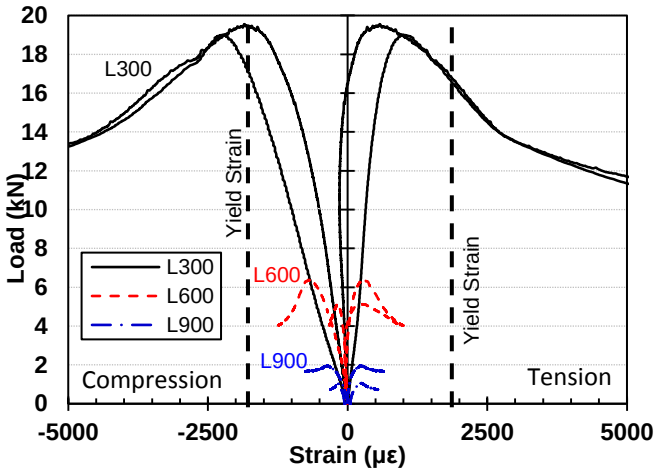

Fig. 10. Load – strain diagram for steel compression tests. Note: two identical specimens tested for each length.

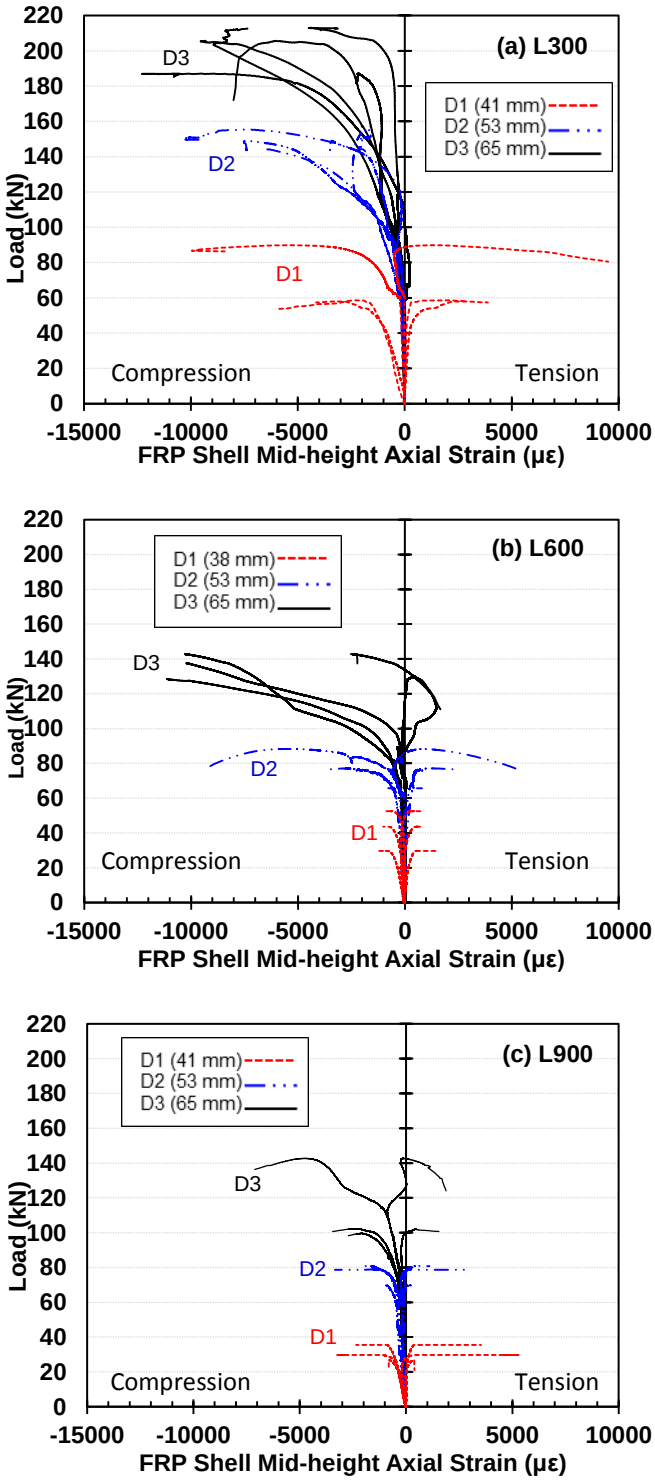

Fig. 11. Load vs axial shell strain diagrams: (a) L300; (b) L600; and (c) L900. Note: three identical specimens tested for each length and diameter.

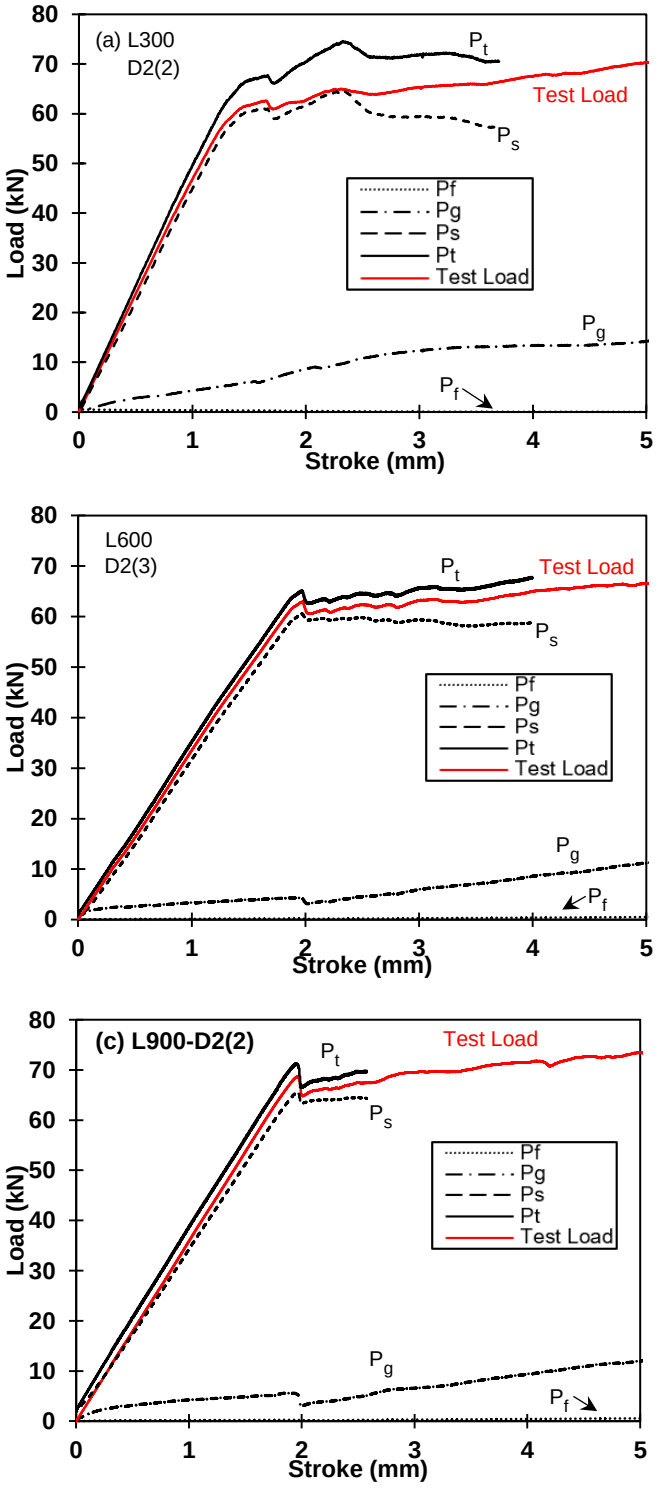

Fig. 12. Sample graphs of contribution of components to load analysis for: (a) L300-D2(2); (b) L600-D2(3); and (c) L900-D2(2).

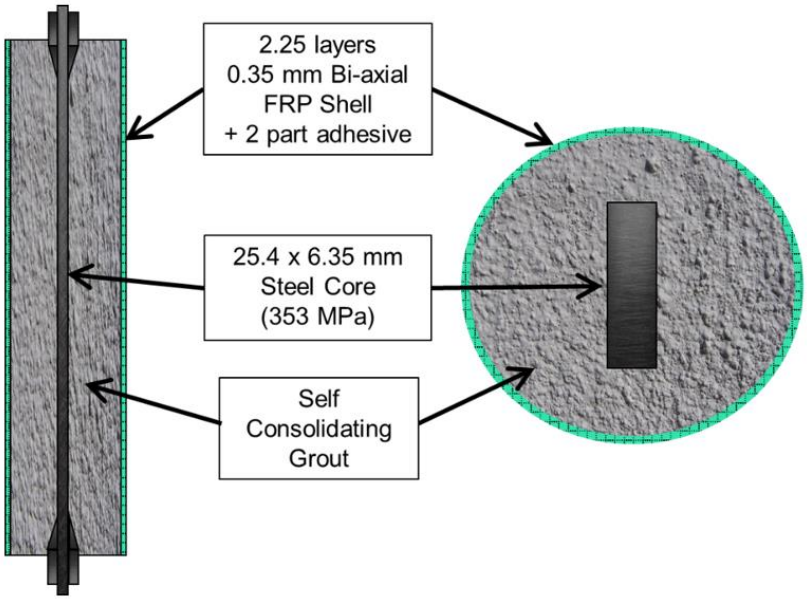

Fig. 13. Cross-section of FRP-BRB specimens for analysis.

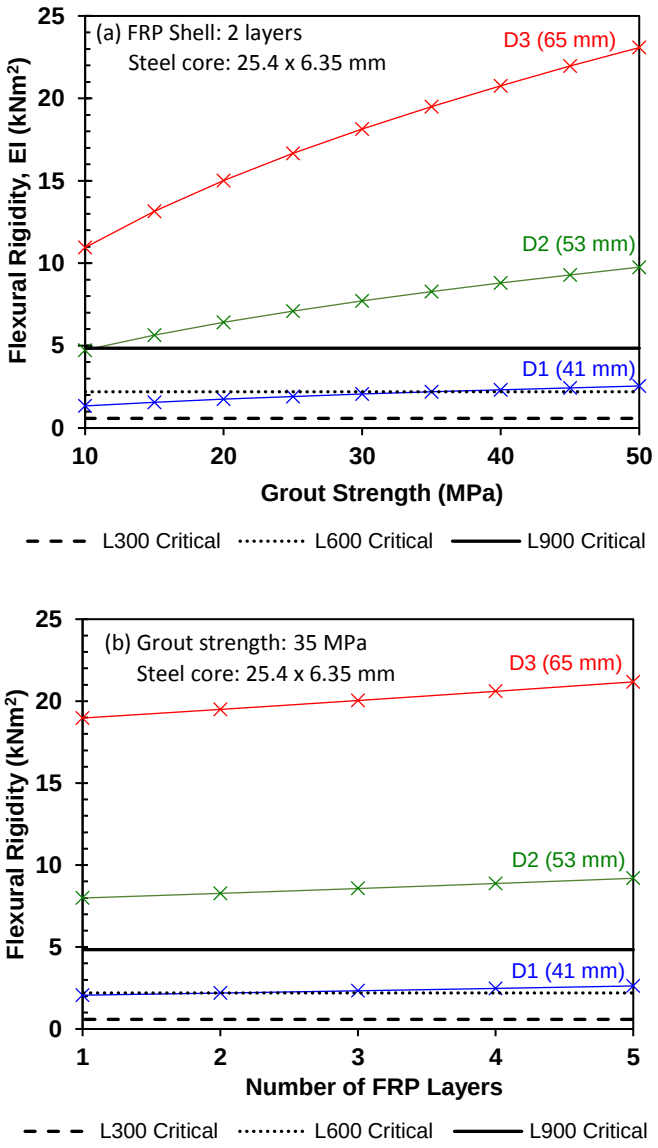

Fig. 14. Parametric study on variation of flexural rigidity of test specimens by changing: (a) grout strength; and (b) number of FRP layers.

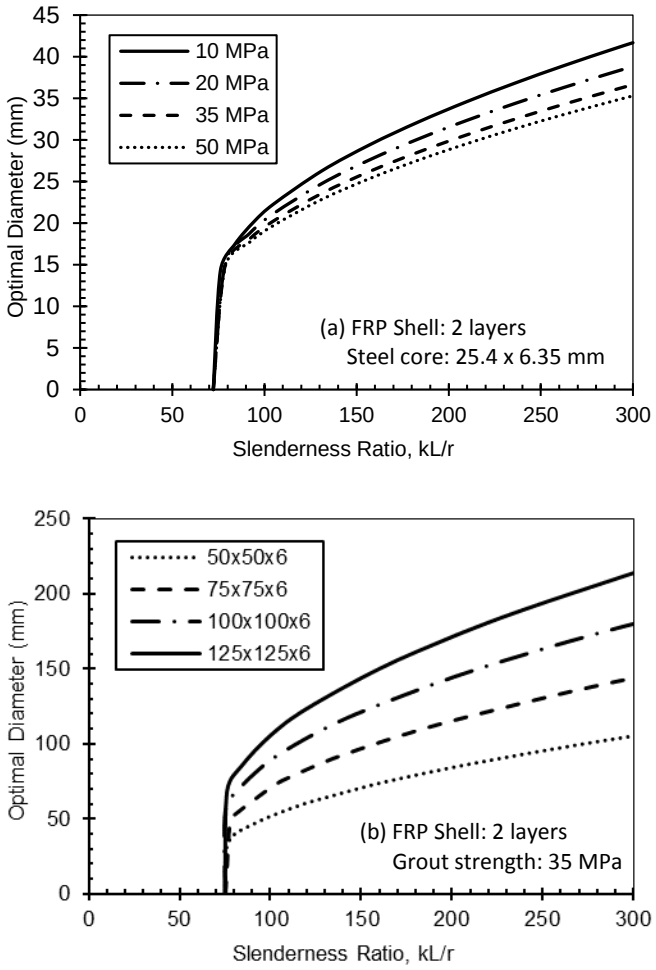

Fig. 15. Parametric study on the effect of slenderness ratio on optimal outer diameter of hybrid system by changing: (a) grout strength; and (b) angle steel core size.